Ion Trapping

Theoretical Minimum

October 31, 2025

Wanxiang Zhang

Personal Note

This is a rather short summary (actually deliberately shortened from another rather short version) of the ideas, calculations and experiments conducted in the literature (listed in the references at the end) regarding ion trap quantum computation. The author will be thankful for any technical or spelling error spotted.

Contents

1 Principles of Ion Traps

1.1 Paul Trap

By Laplace's equation for electric potential in a vacuum (no net charge density):

$$\nabla^2 V = 0 \tag{1}$$

Hence it is impossible to have a naive quadratic potential with positive prefactors in both x and y directions, leading to instability (unbounded motion) in at least one direction. Instead, we must take consideration of either time-varying electric fields (Paul trap) or additional magentic fields (Penning trap) for the purpose of confinement of ions.

A schematic design (electrodes) for a linear Paul-rf trap is shown here:

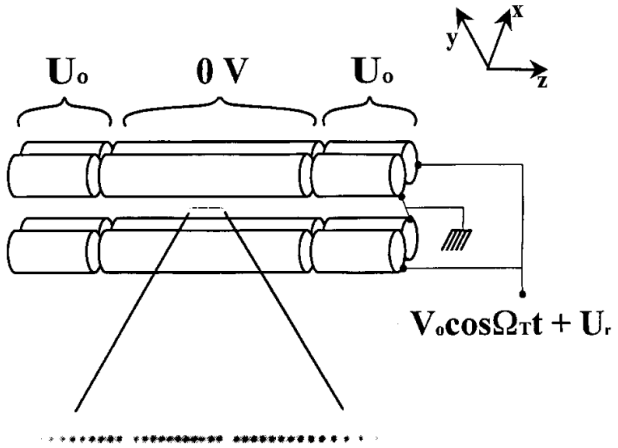

Figure 1: Linear Paul-rf Trap Design [1]

Consider the time-varying potential created by the trap: (near the center and axis of the trap, quadratic approx.)

$$\phi_t = (V_0 \cos(\Omega_T t) + U_r)\left(1 + \frac{x^2 - y^2}{R^2}\right)$$

As well as the static harmonic well:

$$\phi_s = \frac{m}{2q} w_z^2 \left(z^2 - \frac{1}{2}(x^2 + y^2)\right)$$

where $w_z = \sqrt{\frac{2\kappa q U_0}{m z_0^2}}$.
For an ion of charge q, its motion will be dictated by:

$$m\ddot{\boldsymbol{x}} = -q\nabla\phi = -q\nabla(\phi_s + \phi_t) \tag{2}$$

Then one can obtain the simultaneous equations in x and y respectively. Take the x-direction first:

$$\phi = \phi_s + \phi_t = \frac{m}{2q}w_z^2\left(z^2 - \frac{1}{2}(x^2+y^2)\right) + (V_0\cos(\Omega_T t) + U_r)\left(1 + \frac{x^2-y^2}{R^2}\right)$$

$$m\frac{\mathrm{d}^2x}{\mathrm{d}t^2} = -q\left(\frac{mw_z^2}{2q}(-x) + (V_0\cos(\Omega_T t) + U_r)\frac{x}{R^2}\right)$$

$$\frac{\mathrm{d}^2x}{\mathrm{d}t^2} = -\left(\frac{q}{m}(\frac{U_r}{R^2} - \frac{\kappa U_0}{z_0^2}) + \frac{qV_0}{mR^2}\cos(\Omega_T t)\right)x$$

Upon making a substitution of $\zeta = \Omega_T t/2$, we obtain the Mathieu equation(s) (similarly for y), which is a set of simultaneous second-order ordinary differential equations:

$$\frac{\mathrm{d}^2x}{\mathrm{d}\zeta^2} + \left(\underbrace{\frac{4q}{m\Omega_T^2}(\frac{U_r}{R^2} - \frac{\kappa U_0}{z_0^2})}_{a_x} + 2\underbrace{(\frac{2qV_0}{\Omega_T^2 mR^2})}_{q_x}\cos(2\zeta)\right)x = 0 \tag{3}$$

$$\frac{\mathrm{d}^2y}{\mathrm{d}\zeta^2} + \left(\underbrace{-\frac{4q}{m\Omega_T^2}(\frac{U_r}{R^2} + \frac{\kappa U_0}{z_0^2})}_{a_y} + 2\underbrace{(-\frac{2qV_0}{\Omega_T^2 mR^2})}_{q_y}\cos(2\zeta)\right)y = 0 \tag{4}$$

Upon suitable approximations $a_i < q_i^2 << 1$ (where $i = x, y$), the approximate solutions can be given as:

$$\begin{aligned} u_i(t) =& A_i(\cos(\omega_i t + \phi_i)\big[1 + \tfrac{q_i}{2}\cos(\Omega_T t) \\ &+ \tfrac{q_i^2}{32}\cos(2\Omega_T t)\big] + \tfrac{\beta_i q_i}{2}\sin(\omega_i t + \phi_i)\sin(\Omega_T t)) \end{aligned} \tag{5}$$

where $\omega_i = \beta_i\frac{\Omega_T}{2}$, $\beta_i \simeq \left[a_i + \frac{q_i^2}{2}\right]^{1/2}$. Here it is noted that the $\cos(\Omega_T)$ and $\cos(2\Omega_T)$ terms represent the micromotion of ions (undesirable). Under the limit above, the ion beahves as if under a harmonic pseudopotential with frequency (in radial direction) given by:

$$\omega_r = \beta_i\Omega_T/2 \simeq \frac{q_x\Omega_T}{2\sqrt{2}} \tag{6}$$

To produce a "string" of ions linearly along the z axis, it is preferable to have $w_r >> w_z$ to force ions to the axis of the trap.

Note here that w_r is the radial COM vibrational frequency and there are $3L$ normal modes of motion in total (of which L are related to the axial motion).

Albeit the discussion above for quadrupole ion traps seems to be limited to the particular geometry of the '4-rod electrodes' design, the key insight of confinement is generalisable to the other geometries such as blade traps or surface traps, which are more advanced versions of the original scheme.

1.2 Penning Trap

Alternative to the time-varying electric field scheme of a linear Paul trap, one can also consider the Penning trap, which uses purely static fields, with the compensating field being an additional

magnetic field. The electromagnetic fields then constrain the affected ion to move in a predictable periodic way within the allowed range of confinement.

The designs of electrodes are similar to that of a 4-electrode Paul trap but with static fields. The additional insight is an extra axial (z-direction) magnetic field (hard to generate, though) which is strong enough to have a significant impact on ion motion dictated by the Lorentz force.

We start with the following static electric potential:

$$\Phi(x, y, z) = \frac{V_0}{2z_0^2}\left(z^2 - \frac{1}{2}(x^2 + y^2)\right)$$

Under the Lorentz force the EoM can be written as:

$$\begin{pmatrix}\dot{x}\\ \dot{y}\\ \dot{z}\end{pmatrix} = \underbrace{\frac{qB}{m}}_{\omega_c^2}\begin{pmatrix}y\\ -\dot{x}\\ 0\end{pmatrix} + \underbrace{\frac{qV_0}{mz_0^2}}_{\omega_z^2}\begin{pmatrix}x/2\\ y/2\\ -z\end{pmatrix}$$

where ω_c is defined as the free cyclotron frequency and ω_z as the axial frequency.

Without bothering to the trivial detail here, one can eventually obtain two frequencies of oscillations with the solution to a quadratic form:

$$\omega_\pm = \frac{1}{2}\left(\omega_c \pm \sqrt{\omega_c^2 - 2\omega_z^2}\right) \tag{7}$$

where ω_+ is the (faster) modified cyclotron frequency (but essentially very close to the free cyclotron frequency for $\omega_z << \omega_c$), and ω_- is the slower magnetron frequency.

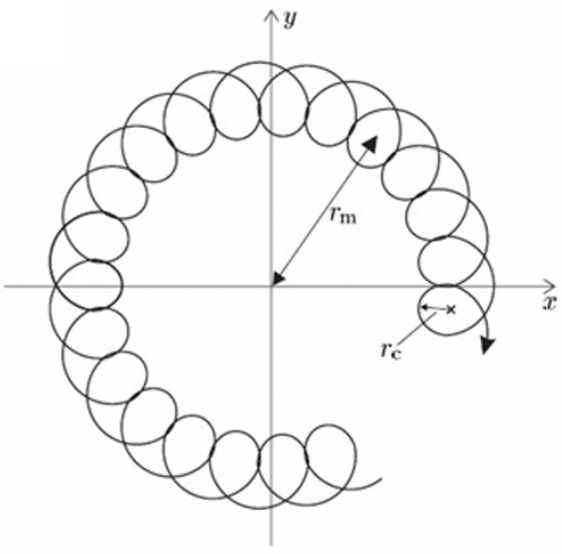

Figure 2: Ion Trajectory in Penning Traps [13]

For real stable solutions, one needs to fulfill the requirement that $\omega_c^2 > 2\omega_z^2$, which is equivalent to

a condition on the magnitude of the magnetic flux density:

$$B > \sqrt{\frac{2mV_0}{qz_0^2}} \tag{8}$$

which is expected since in the opposite case the magnetic field is too small that the ion particle simply falls down the saddle-shaped static electric potential implying failure of confinement.

The two frequencies in (7) can be illustrated in a rough trajectory plotted as in *Figure 2*. The large circle is the result of motion under magnetron frequency while the fast local oscillations are due to (modified) cyclotron frequency.

2 Quantum Mechanics of Ions

2.1 Motional and Internal States

Following some ingenious experimental schemes to realise ion trapping, we return back to theories formulating the states of trapped ions. It is, to a good approximation for near-quadratic potentials, to describe the motion of a single trapped ion with the Hamiltonian of a standard quantum harmonic oscillator:

$$\hat{H}_{osc} = \hbar\omega_i \hat{n}_i \tag{9}$$

where $\hat{n}_i = a_i^\dagger a_i$ and is the number operator, whilst a_i is the (lowering) ladder operator. Thus one can deduce the position operator $\hat{z}$ (in z direction) by adding the lowering operator with the raising operator:

$$a + a^\dagger = \sqrt{\frac{m\omega}{2\hbar}}\left(\hat{z} + \frac{i}{mw}\hat{p}\right) + \sqrt{\frac{m\omega}{2\hbar}}\left(\hat{z} - \frac{i}{mw}\hat{p}\right) = \sqrt{\frac{2m\omega}{\hbar}}\hat{z}$$

Hence

$$\hat{z} = \underbrace{\sqrt{\frac{\hbar}{2m\omega}}}_{z_0}\left(a + a^\dagger\right) \tag{10}$$

$z_0 = \sqrt{\frac{\hbar}{2m\omega}}$ is the approximate spread of the zero-point wavefunction. For a typical $^9Be^+$ ions in a trap where $\omega_z/(2\pi) = 10\,\text{MHz}$, we have $z_0 = 7.5\,\text{nm}$.

Thus it follows that the motional wavefunction (pure state assumed) of one mode can be written as a superposition of the SHO states:

$$\begin{aligned}\Psi_{motion} &= \sum_{n=0}^{\infty} c_n \exp\left(\frac{-iE_n t}{\hbar}\right)|n\rangle = \sum_{n=0}^{\infty} c_n \exp\left(\frac{-i(\hbar\omega_i n)t}{\hbar}\right)|n\rangle \\ &= \sum_{n=0}^{\infty} c_n \exp(-in\omega_i t)\,|n\rangle\end{aligned} \tag{11}$$

If we are only interested in the first two terms (for qubit applications), taking the simple form $c_0\,|0\rangle + c_1 \exp(-iw_1 t)\,|1\rangle$ is sufficient.

As with most spin-1/2 systems, it is appropriate to approximate a spin-1/2 magnetic moment under the influence of a (fictitious) magnetic field, to represent this "two-level" ion:

$$H_{internal} = -\boldsymbol{\mu}\cdot\boldsymbol{B} = -\mu_M S_z B_0 = \hbar(-\frac{\mu_M B_0}{\hbar})S_z = \hbar\omega_0 S_z \tag{12}$$

Typically we expect the internal resonant frequency to be much larger than any motional mode frequency ($\omega_0 >> \omega_z$).

Given that there are two levels $E_\uparrow = \hbar\omega_0/2$ and $E_\downarrow = -\hbar\omega_0/2$. We can write down the internal state wavefunction:

$$\begin{aligned}\Psi_{internal} &= C_\downarrow \exp(-iE_\downarrow t/\hbar)\,|\downarrow\rangle + C_\uparrow \exp(-iE_\uparrow t/\hbar)\,|\uparrow\rangle \\ &= C_\downarrow \exp(i\omega_0 t/2)\,|\downarrow\rangle + C_\uparrow \exp(-i\omega_0 t/2)\,|\uparrow\rangle\end{aligned} \tag{13}$$

In these experiments, measurement is performed using a laser beam that is carefully polarized and tuned to a specific atomic transition. This setup creates what's known as a "cycling" transition, where an atom in one internal state will scatter many photons while an atom in the other state scatters virtually none. By detecting even a modest number of these photons, we can achieve near-perfect (approaching 100%) discrimination efficiency between the two atomic states. Generally for $n_d > 10$ (number of photons), detection will be highly efficient, with probability of error $\sim 10^{-44}$. The detail would be discussed again by the end of the chapter.

2.2 Interaction and Coupling with Fields

Consider the situations where fields resonantly drive transitions between internal or motional states and when they drive transitions between these states simultaneously (entanglement). Start with the interaction Hamiltonian: (magnetic coupling)

$$H_1 = -\boldsymbol{\mu_d} \cdot \boldsymbol{B} \tag{14}$$

Given that

$$\begin{aligned} \boldsymbol{\mu_d} &= \mu_M \boldsymbol{S} \\ \boldsymbol{B} &= B_1 \cos(kz - \omega t + \phi)\hat{\boldsymbol{x}} \end{aligned}$$

Substitute to get:

$$\begin{aligned} H_1 &= -\mu_M S_x B_1 \cos(kz - \omega t + \phi) \\ &= -\mu_M \frac{(S_+ + S_-)}{2} B_1 \frac{\exp(i(kz - \omega t + \phi)) + \exp(-i(kz - \omega t + \phi))}{2} \\ &= \underbrace{-\frac{\mu_M B_1}{4}}_{\hbar\Omega} (S_+ + S_-) \left(\exp(i(kz - \omega t + \phi)) + \exp(-i(kz - \omega t + \phi))\right) \\ &= \hbar\Omega (S_+ + S_-)(\exp(i(kz - \omega t + \phi)) + \exp(-i(kz - \omega t + \phi))) \end{aligned} \tag{15}$$

Throughout the calculations, we will negletc terms with fast oscillations (rotating-wave approximation, neglecting $\exp(\pm i(\omega + \omega_0)t)$ or higher-frq terms). Also note that in some literature [5], the prefactor has a 1/2 which is due to a different definition of $\hbar\Omega = \mu_M B_1/2$.

The general wavefunction is entangled between the two degrees of freedom (internal and motional), and can be written as a superposition of product states (but its entirety is not necessarily a product state):

$$\Psi = \sum_{M_z=\downarrow,\uparrow} \sum_{n=0}^{\infty} C_{M_z,n}(t) \left|M_z\right\rangle \left|n\right\rangle \tag{16}$$

In the Heisenberg picture, considering the evolution of the hamiltonian $H_1 \to H_1' = U_0^\dagger(t) H_1 U_0(t)$, where $U_0(t) = \exp\left(-i\left(\frac{H_0}{\hbar}\right)t\right) = \exp(-i\omega_0 t)$. Note also that $kz = kz_0(ae^{-i\omega_z t} + a^\dagger e^{i\omega_z t})$.

THe Hamiltonian is hence calculated by:

$$H_1' = \hbar\Omega(S_+ \exp(i\omega_0 t) + S_- \exp(-i\omega_0 t))[\exp(i(kz - \delta t + \phi)) + \exp(-i(kz - \delta t + \phi))]$$

Simlifying to get:

$$H_1' = \hbar\Omega S_+ \exp\left(i\left[\eta(ae^{-i\omega_z t} + a^\dagger e^{i\omega_z t}) - \delta t + \phi\right]\right) + \text{h.c.} \tag{17}$$

where $\delta \equiv \omega - \omega_0$, and $\eta \equiv kz_0$ is the Lamb-Dicke parameter, characterizing the coupling strength between an ion's internal states and its motional states. For resonant transitions, $\delta \simeq \omega_z(n' - n)$ where n' and n are integers.

2.3 Rabi Oscillation

The coefficients $C_{\uparrow,n'}$ and $C_{\downarrow,n}$ for Ψ can be solved effectively through simultaneous 1st-order (time-wise) differntial equations (detail omitted), resulting in Rabi Oscillations between the states $|\uparrow, n'\rangle$ and $|\downarrow, n\rangle$. The superposition state is defined as $|\psi\rangle = C_{\downarrow,n}|\downarrow, n\rangle + C_{\uparrow,n'}|\uparrow, n'\rangle = \left[C_{\uparrow,n'}, C_{\downarrow,n}\right]^T$, so considering just the time-evolution matrix entries of the resonant case:

$$\Psi(t) = \begin{bmatrix} \cos\left(\Omega_{n',n}t\right) & -ie^{i\left[\phi+\frac{\pi}{2}|n'-n|\right]}\sin\left(\Omega_{n',n}t\right) \\ -ie^{-i\left[\phi+\frac{\pi}{2}|n'-n|\right]}\sin\left(\Omega_{n',n}t\right) & \cos\left(\Omega_{n',n}t\right) \end{bmatrix} \Psi(0) \tag{18}$$

where the Rabi frequencies are given as

$$\Omega_{n',n} \equiv \Omega \left| \left\langle n' \middle| e^{i\eta(a+a^\dagger)} \middle| n \right\rangle \right| \tag{19}$$

A special case is when the Lamb-Dicke limit is satisfied, where the amplitude of the ion's motion in the direction of radiation is much less than $\lambda/2\pi$, or equivalently:

$$\langle \Psi_{motion}| \, k^2 z^2 \, |\Psi_{motion}\rangle^{1/2} << 1 \tag{20}$$

A less strict condition is where $\eta << 1$ which is true if the Lamb-Dicke limit is satisfied, but the converse isn't guaranteed. When the Lamb-Dicke limit is satisfied, the Hamiltonian in (17) can be expanded to:

$$H_1' \simeq \hbar\Omega S_+(1 + i\eta(ae^{-i\omega_z t} + a^\dagger e^{i\omega_z t}))\exp(i(-\delta t + \phi)) + \text{h.c.} \tag{21}$$

There are three types of useful transitions: the carrier ($n' = n, |g, n\rangle \to |e, n\rangle$), the first red sideband ($n' = n–1, |g, n\rangle \to |e, n-1\rangle$), and the first blue sideband ($n' = n+1, |g, n\rangle \to |e, n+1\rangle$) whose Rabi frequencies, in the Lamb-Dicke limit, are given by Ω, $\eta\sqrt{n}\Omega$ and $\eta\sqrt{n+1}\Omega$ respectively.

e.g. Take the case of red sideband where $\delta = -\omega_z$ and $\phi = -\frac{\pi}{2}$, then equation (21) further simplifies:

$$\begin{aligned} H_1' &\simeq \hbar\Omega S_+(1 + i\eta(ae^{-i\omega_z t} + a^\dagger e^{i\omega_z t}))\exp(i(\omega_z t - \pi/2)) + \text{h.c.} \\ &\simeq \hbar\Omega S_+ i\eta a \exp(-i\pi/2) + \text{h.c.} \\ &\simeq \hbar\eta\Omega(S_+ a + S_- a^\dagger) \end{aligned} \tag{22}$$

This Hamiltonian is the same as the "Jaynes-Cummings Hamiltonian" in QED, describing the coupling of a two-level atom to a single mode of the (quantized) radiation field. Hence driving transitions between states will create entanglement between the internal and motional states, providing basis for two-qubit quantum logic gates.

For clarity, the Hamiltonians of the sidebands (red & blue) and the carrier cases could be expanded (in the Lamb-Dicke regime) in the following forms:

$$H_{rsb} \simeq \frac{\hbar\eta\Omega}{2}(\sigma_+ a e^{i\phi} + \sigma_- a^\dagger e^{-i\phi}) \tag{23}$$

$$H_{car} \simeq \frac{\hbar\eta\Omega}{2}(\sigma_+ e^{i\phi} + \sigma_- e^{-i\phi}) \tag{24}$$

$$H_{bsb} \simeq \frac{\hbar\eta\Omega}{2}(\sigma_+ a^\dagger e^{i\phi} + \sigma_- a e^{-i\phi}) \tag{25}$$

where $S_\pm = \sigma_\pm/2$ and $\omega_z = \nu$ is the harmonic oscillator frequency.

2.4 Stimulated Raman Transitions

A schematic setup is shown in *Figure 3*.

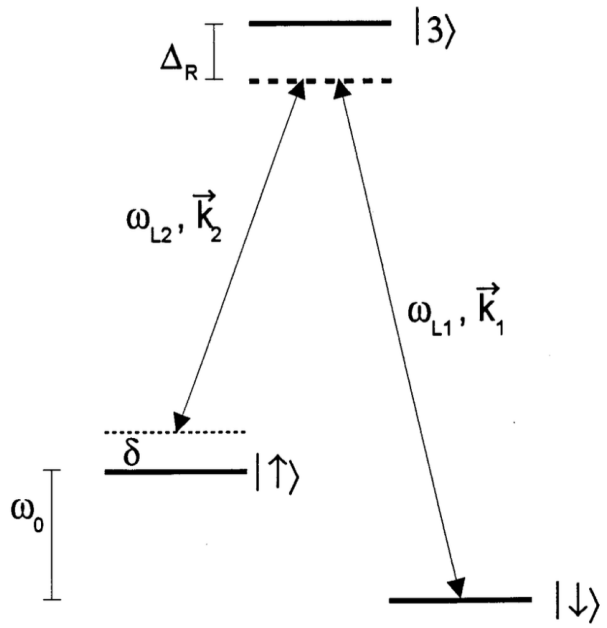

Figure 3: Stimulated-Raman Transitions

The relevant Hamiltonian, replaced from (15), is given by:

$$H_1 = \hbar\Omega(S_+ + S_-)(\exp(i[(\boldsymbol{k_1} - \boldsymbol{k_2}) \cdot \boldsymbol{x} - (\omega_{L1} - \omega_{L2})t + \phi]) + \text{h.c.}) \tag{26}$$

The transition is driven between state $|\uparrow\rangle$ and $|\downarrow\rangle$ through another state $|3\rangle$ by stimulated-Raman transitions using plane EM waves (typically considering electric dipole transitions). It is possible to calculate theoretically the wavefunctions in the Schrödinger picture as well as calculating the matrix elements through a set of simultaneous 1st-order differential equations. An optical Stark shift should also be included, but may be neglected if the shifts are made equal for $|\uparrow\rangle$ and $|\downarrow\rangle$ since no additional phase shifts caused.

The mathematics involved would be the same as for a two-level system if one makes the difference between wavevectors/relative phases approximately equal to the wavevector/relative phase discussed before in the original Hamiltonian (15). More detail can be found in the paper by Wineland et al. [1]

2.5 Open Quantum Systems

So far our discussion has been limited to assuming a closed quantum system which is an idealisation of real systems. In reality, we mostly only treat (sub)systems which interact with the environment. We thus unavoidably need a formulation of Open Quantum Theory which can deduce the equations

of motion of the reduced systems from the total system (with environment).

The Lindblad Master Equation [10] describes the quantum dynamics of a subsystem of interest separated from the environment of the more complicated total system (the simplest case with only one relevant frequency considered).

$$\frac{d}{dt}\rho(t) = -i\left[H + H_{\text{int}}(t), \rho(t)\right] + \sum_n \left(L_n \rho(t) L_n^\dagger - \frac{1}{2}\left\{ L_n^\dagger L_n, \rho(t) \right\} \right) \tag{27}$$

where the operators L_n are the jump operators associated with decoherence and noise from interaction with the environment, H and $H_{int}(t)$ are the Hamiltonians of the subsystem (of interest) and the coupling (with the environment) respectively, and $\rho(t)$ is the density operator describing the state of interest. Each n is associated with one channel of possible decoherence.

For numerical simulations, we model $L_n = \sqrt{\gamma_n} A_n$ where A_n is the coupling (between the system and the environment) operator while γ_n is the corresponding rate.

Though formulated mathematically, it is still hard to solve a particular system with the Master equation by hand analytically. However, one can numerically solve a time-evolutionary problem in this way, such as tackling the standard Rabi oscillation discussed before, which certainly occurs experimentally under some (probably undesirable) interactions with the environment. It is worthwhile to note that even though calculations based on the traditional Schrödinger equation are usually more efficient, the Master equation should be applied for better accuracy when the coupling with environment is not negligible.

3 Experimental Implementation

3.1 Initialisation and Cooling

For preparation of ions in the ground state ($|n=0\rangle$ motional state) in initilisation. A combination of Doppler cooling and sideband laser cooling is used.

Doppler cooling is achieved in the following way: an atom moving toward a laser beam has transition frequencies which are slightly higher in energy than an atom moving away. If the laser is tuned (red-detuned) such that it is absorbed only by approaching atoms, then the atoms slow down (lose momentum) because the photons kick them in the opposite direction (for emission it is roughly isotropic so the net effect is determined by just the absorption preference). Doppler cooling usually only cools to a temperature of about 1 mK (Doppler cooling limit), so sideband cooling is necessary.

The basic idea of sideband cooling is very simple: a laser is used to excite atoms which are in any state other than the desired initial state into some high-energy state, and combined with random relaxation processes this leads to preferential population of the desired state. [3]

In the schematic diagram *Figure 4*, the cooling process is achieved by the folowing sequence: $|\downarrow\rangle|n\rangle \underbrace{\rightarrow}_{a} |\uparrow\rangle|n-1\rangle \underbrace{\rightarrow}_{b} |\downarrow\rangle|n-1\rangle$. Part (a) is induced by a stimulated-Raman transition tuned to the first red sideband. In part (b), a third laser pumps the state to the higher auxiliary state which then spontaneously decays and partially results in a spin-down lower motional state (this is highly efficient even if sometimes it pumps back to the spin-up state originally) The process is then repeated until we reduce to the ground state.

This only shows the traditional laser-based manipulations for logic gate controls. However, microwave or electronically-based techniques are also possible to realise quantum logic gate operations, albeit facing a key challenge in individual addressing (discussed in the following section). Moreover, another useful method applied widely is the EIT cooling [12] which involves a 3-level system. The detail is rather involved, but the key is that the detuning is chosen such that the atomic system is pumped to a dark state not coupled to the laser fields, thus significantly decreasing the rate of spontaneous emissions (hence intrinsic heating processes). The general advantage is thus that EIT cooling substantially shortens the cooling time to reach ground states over a range of oscillation frequencies compared to sideband cooling. It also relies on a more robust cooling technique with a smaller number of optimization parameters.

3.2 Quantum Logic Gates

Single-bit rotations can be characterized by the following unitary operator:

$$R(\theta,\phi) = \begin{bmatrix} \cos(\theta/2) & -ie^{i\phi}\sin(\theta/2) \\ -ie^{-i\phi}\sin(\theta/2) & \cos(\theta/2) \end{bmatrix} \tag{28}$$

Where we have started from the transformation of (18), setting $n' = n$ and $\theta = 2\Omega_{n',n}t$. This is equivalent to applying an oscillating magnetic field in the x direction for the spin-1/2 model. From different parameter choices we can obtain the desired single-qubit unitary gates such as the standard Pauli gates, Hadamard, etc.

For universal computing it is also necessary to consider the implementation of 2-qubit entangling

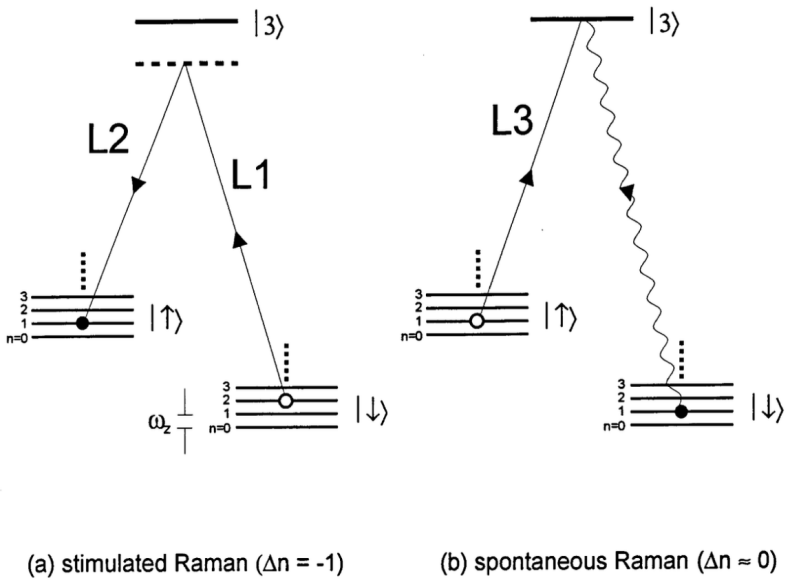

Figure 4: Sideband Laser Cooling

gates (i.e. CNOT or CZ gates). This can be implemented by the Cirac-Zoller CZ scheme [8], or using the more advanced Mølmer–Sørensen (MS) gate [9].

The Cirac-Zoller scheme utilises the standard coupling of the internal energy levels of the n-th ion ($|g\rangle_n, |e_0\rangle_n, |e_1\rangle_n$,...), the CM motional modes ($|0\rangle, |1\rangle, ...$) shared by all ions. Manipulations using red-sideband lasers are described by the Hamiltonian as in (22). Considering the interaction between $|g\rangle_n$ and $|e_q\rangle_n$ (where n specifies the selected ion and q is the polarization number), since $S_+ = \sigma_+/2 = |e_q\rangle_n \langle g|/2$ and $S_- = |g\rangle_n \langle e_q|/2$, the Hamiltonian can be written as:

$$H_{n,q} = \frac{\hbar\eta\Omega}{2}\left(|e_q\rangle_n \langle g| a + |g\rangle_n \langle e_q| a^\dagger\right) \tag{29}$$

(where we have neglected the prefactor $1/\sqrt{N}$ which is irrelevant for the core physics here)

To proceed, we may write the unitary operator $U = \exp(-iHt/\hbar)$ with the time focused by laser beam chosen as $t = k\pi/(\Omega\eta)$ (i.e. $k\pi$ pulse):

$$U_n^{k,q} = \exp\left[-ik\frac{\pi}{2}\left(|e_q\rangle_n \langle g| a + |g\rangle_n \langle e_q| a^\dagger\right)\right] \tag{30}$$

To actually implement the Cirac-Zoller CZ gate, we choose the control qubit to be the m-th ion, while the target qubit to be the n-th ion, both interacted with the CM motional modes $|0\rangle, |1\rangle, ...$ and initialised at the ground motional state $|0\rangle$ (which is actually a rather strict condition requiring very low temperatures and avoided by the Mølmer-Sørensen gate). To illustrate the calculations,

the following results can be very helpful:

$$
\begin{aligned}
U_n^{1,0} |g\rangle_n |0\rangle &= \exp(0) |g\rangle_n |0\rangle = |g\rangle_n |0\rangle \\
U_n^{1,0} |g\rangle_n |1\rangle &= -i \sin(\pi/2)(|e_0\rangle_n \langle g|g\rangle)(a |1\rangle) = -i |e_0\rangle_n |0\rangle \\
U_n^{1,0} |e_0\rangle_n |0\rangle &= -i \sin(\pi/2)(|g\rangle_n \langle e_0|e_0\rangle)(a^\dagger |0\rangle) = -i |g\rangle_n |1\rangle \\
U_n^{2,1} |g\rangle_n |0\rangle &= \exp(0) |g\rangle_n |0\rangle = |g\rangle_n |0\rangle \\
U_n^{2,1} |g\rangle_n |1\rangle &= \cos(\pi) |g\rangle_n |1\rangle = - |g\rangle_n |1\rangle \\
U_n^{2,1} |e_0\rangle_n |0\rangle &= \exp(0) |e_0\rangle_n |0\rangle = |e_0\rangle_n |0\rangle \\
U_n^{2,1} |e_0\rangle_n |1\rangle &= \exp(0) |e_0\rangle_n |1\rangle = |e_0\rangle_n |1\rangle
\end{aligned}
$$

Thus, if we apply unitary evolutions in the order of $U_m^{1,0} U_n^{2,1} U_m^{1,0}$ on the possible initialised states, the CZ gate can be constructed as:

$$
C_Z = U_m^{1,0} U_n^{2,1} U_m^{1,0} = \begin{pmatrix} 1 & 0 & 0 & 0 \\ 0 & 1 & 0 & 0 \\ 0 & 0 & 1 & 0 \\ 0 & 0 & 0 & -1 \end{pmatrix} \tag{31}
$$

where the basis for this matrix is $\{|g\rangle_m |g\rangle_n |0\rangle, |g\rangle_m |e_0\rangle_n |0\rangle, |e_0\rangle_m |g\rangle_n |0\rangle, |e_0\rangle_m |e_0\rangle_n |0\rangle\}$, and the entries can be verified easily.

Trivially, it followed that applying HC_ZH is equivalent to a standard CNOT entangling gate. In fact, any non-trivial entangling two-qubit gate (in combination with single-qubit gates) would suffice for universal computation.

As characterised by the calculations, the Cirac-Zoller scheme requires two strict conditions: (i) individual addressing of a particular pair of ions. (ii) very low temperature to ensure the motional state is initialised at $|0\rangle$. These can be very unpractical, so an improved method for 2-qubit entangling gate, the Mølmer-Sørensen gate, is more useful currently.

The Mølmer-Sørensen scheme is outlined in *Figure 5*. For two ions chosen, lasers are used to couple the states $|ggn\rangle \leftrightarrow \{|egn+1\rangle, |gen-1\rangle\} \leftrightarrow |een\rangle$, through a combination of red or blue sidebands. However, the lasers are particularly detuned from the sidebands such that no populations can be gained in the intermediate states $\{|egn+1\rangle, |gen-1\rangle\}$ as they are kept off-resonant.

It is mathematically possible to show, via standard second-order perturbation theory, by restricting the intermediate states considered to $\{|egn+1\rangle, |gen-1\rangle\}$, that the equivalent frequency of oscillations $\tilde{\Omega}$ between states $|gg\rangle$ and $|ee\rangle$ is given by:

$$
\tilde{\Omega} = -\frac{(\Omega\eta)^2}{2(\nu - \delta)} \tag{32}
$$

where $\delta = \omega_1 - \omega_{eg}$ is the small detuning of the laser, assuming both ions with the same Lamb-Dicke parameter η and Rabi frequency Ω.

The fundamental importance of (32) is the independence of n (mathematically due to a difference of two terms with factor $n+1$ and n respectively), which means the evolution of internal

states of the ions is insensitive to the vibrational quantum numbers, so any mixture of superposition of vibrational states (phonon number) is allowed for this interaction. Additionally, this does not limit to the pair of $\{|gg\rangle, |ee\rangle\}$, as $\{|ge\rangle, |eg\rangle\}$ can also be entangled by the same mechanics.

In practice, one applies laser detuned with $\pm\delta$ to both ions continuously, so there will be two more paths in addition to the two paths outlined in *Figure 5*. The physics is only changed by multiplying (32) by a factor of 2. The unitary evolution operator for the two-ion states can be described by the following:

$$
\begin{aligned}
|gg\rangle &\to \cos\left(\frac{\tilde{\Omega}T}{2}\right)|gg\rangle + i\sin\left(\frac{\tilde{\Omega}T}{2}\right)|ee\rangle \\
|ee\rangle &\to \cos\left(\frac{\tilde{\Omega}T}{2}\right)|ee\rangle + i\sin\left(\frac{\tilde{\Omega}T}{2}\right)|gg\rangle \\
|ge\rangle &\to \cos\left(\frac{\tilde{\Omega}T}{2}\right)|ge\rangle - i\sin\left(\frac{\tilde{\Omega}T}{2}\right)|eg\rangle \\
|eg\rangle &\to \cos\left(\frac{\tilde{\Omega}T}{2}\right)|eg\rangle - i\sin\left(\frac{\tilde{\Omega}T}{2}\right)|ge\rangle
\end{aligned}
$$

This is sufficient for a non-trivial entangling gate. For example, setting $\tilde{\Omega}T/2 = \pi/4$, one reads $|gg\rangle \to \frac{1}{\sqrt{2}}(|gg\rangle + i\,|ee\rangle)$, which is a maximally-entangled state evolved from a product state $|gg\rangle$.

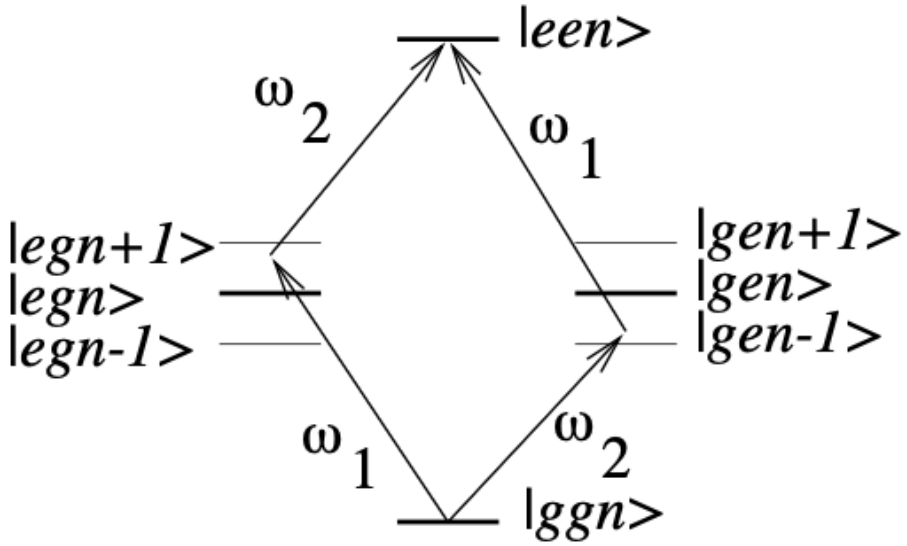

Figure 5: Laser Detuning for MS Gate [9]

3.3 Detection of Internal States

As with all quantum mechanical states, the unitary evolution of states contains quantum information which is valuable but nonetheless obscure to an observer. For physical implementation we also

need a scheme for measurement which accurately returns the eigenstate of the measured outcome.

This is not hard to achieve with lasers: we may tune the beam to specifically trigger a stimulated transition with a third state (which quickly decays back to $|0\rangle$, say), leading to detectable fluorescence. But there will be no scattered photons to the other state (i.e. $|1\rangle$). Hence if we detect for a sufficient amount of photons it will be possible to ensure accurate measurement of state ($|0\rangle$ or $|1\rangle$), as well as the corresponding probability (amplitude norm squared) if the state is in a general superposition in this basis.

4 Relevant Sources

(Those labeled with † are particularly helpful)

[1]† Wineland, D. J., Monroe, C., Itano, W. M., Leibfried, D., King, B. E., & Meekhof, D. M. (1998). Experimental issues in coherent quantum-state manipulation of trapped atomic ions. Journal of research of the National Institute of Standards and Technology, 103(3), 259.
[2] Smith, M. C., Leu, A. D., Gely, M. F., & Lucas, D. M. (2024). Individually Addressed Quantum Gate Interactions Using Dynamical Decoupling. PRX Quantum, 5(3), 030321.
[3]† Jones, J. A., & Jaksch, D. (2012). Quantum Information, Computation and Communication. Cambridge: Cambridge University Press.
[4] Ospelkaus, C., Langer, C. E., Amini, J. M., Brown, K. R., Leibfried, D., & Wineland, D. J. (2008). Trapped-ion quantum logic gates based on oscillating magnetic fields. Physical review letters, 101(9), 090502.
[5]† Nielsen, M. A., & Chuang, I. L. (2010). Quantum computation and quantum information. Cambridge university press.
[6] Weber, M. A., Löschnauer, C., Wolf, J., Gely, M. F., Hanley, R. K., Goodwin, J. F., ... & Lucas, D. M. (2023). Cryogenic ion trap system for high-fidelity near-field microwave-driven quantum logic. Quantum Science and Technology, 9(1), 015007.
[7] COMSOL Inc. COMSOL Multiphysics®. v. 6.2.
[8] Cirac, J. I., & Zoller, P. (1995). Quantum computations with cold trapped ions. Physical Review Letters, 74(20), 4091–4094.
[9] Sørensen, A., & Mølmer, K. (1999). Quantum computation with ions in thermal motion. Physical Review Letters, 82(9), 1971–1974.
[10] Manzano, D. (2020). A short introduction to the Lindblad master equation. Aip advances, 10(2).
[11] Lambert, N., Giguère, E., Menczel, P., Li, B., Hopf, P., Suárez, G., Gali, M., Lishman, J., Gadhvi, R., Agarwal, R., Galicia, A., Shammah, N., Nation, P., Johansson, J. R., Ahmed, S., Cross, S., Pitchford, A., & Nori, F. (2024). QuTiP 5: The Quantum Toolbox in Python. arXiv.
[12] Lechner, R., Maier, C., Hempel, C., Jurcevic, P., Lanyon, B. P., Monz, T., ... & Roos, C. F. (2016). Electromagnetically-induced-transparency ground-state cooling of long ion strings. Physical Review A, 93(5), 053401.
[13]† Foot, C. J. (2005). Atomic physics (Vol. 7). Oxford University Press.